Description of the multidimensional potential-energy surface in fission of ^{252}Cf and ^{258}No

A. Zdeb [1,2,*] M. Warda [3,†] and L. M. Robledo [4,5,‡]

[1]*CEA, DAM, DIF, F-91297 Arpajon, France*
[2]*Université Paris-Saclay, CEA, LMCE, F-91680 Bruyères-le-Châtel, France*
[3]*Instytut Fizyki, Uniwersytet Marii Curie–Skłodowskiej, PL-20031 Lublin, Poland*
[4]*Departamento de Física Teórica and CIAFF, Universidad Autónoma de Madrid, Madrid, Spain*
[5]*Center for Computational Simulation, Universidad Politécnica de Madrid, Campus de Montegancedo, Bohadilla del Monte, E-28660 Madrid, Spain*

Microscopic studies of nuclear fission require the evaluation of the potential-energy surface as a function of the collective coordinates. A reasonable choice of constraints on multipole moments should be made to describe the topography of the surface completely within a reasonable amount of computing time. We present a detailed analysis of fission barriers in the self-consistent Hartree-Fock-Bogoliubov approach with the D1S parametrization of the Gogny nucleon-nucleon interaction. Two heavy isotopes representing different spontaneous fission modes, ^{252}Cf (asymmetric) and ^{258}No (bimodal), have been chosen for the analysis. We have shown the existence of complicated structures on the energy surface that cannot be fully described in two-dimensional calculations. We analyze apparent problems that can be encountered in this type of calculations: multiple solutions for given constraints and transitions between various overlapping potential-energy surfaces. These issues may be partially solved by the analysis of the potential-energy surface spanned by triple constraints, but even in this case one may find multiple solutions and surface discontinuities. Analysis of the potential-energy surface in two dimensions is often very successful but it must be carried out with special attention to possible discontinuities.

I. INTRODUCTION

The accurate description of collective nuclear motion from the ground state up to the scission point represents a crucial step to understand the fission of an atomic nucleus. An essential ingredient is the behavior of the binding energy of the nucleus as a function of the parameters characterizing the collective degrees of freedom. On its way from the initial ground state configuration to scission, the nucleus has to tunnel through a potential-energy barrier determining the timescale of fission half-lives. Not only the height but also the width and the shape of the fission barrier are important for spontaneous fission half-life estimations, while the topography of the potential-energy surface (PES) is essential to determine fission dynamics. A detailed description of the theory of fission and challenges in this field can be found in the review papers [1–3].

Many theoretical papers describing the PES in heavy actinides have been published recently, improving our knowledge of fission in heavy and superheavy nuclei [4–24]. In those articles, one can distinguish two different approaches to describe the evolution of the shape of the nucleus on its way from the initial configuration towards scission. Both are based on the assumption that the most probable (one-dimensional) path in the considered deformation space is the one connecting the lowest energy points along the path. In the first approach, which is mostly used with macroscopic-microscopic theories, a predefined class of nuclear shapes defined uniquely in terms of a given set of deformation parameters is used to define the set of accessible configurations to be used in the characterization of the energy. The number of deformation parameters defines the dimensionality of the problem. An increasing number of dimensions enlarges the variety of shapes used and, therefore, usually improves the calculation's quality by providing lower energy solutions. This flexibility comes at the expense of calculating the energy for a huge number of points in the deformation space. On the other hand, the approach benefits from full control over the shapes characterizing the evolution of the nucleus from the ground state to scission. The alternative approach is mostly based on microscopic self-consistent methods. In the self-consistent procedure, the wave functions along the fission path are determined by the minimization of the energy of the nucleus within a given set of constraints and assumed symmetries. There are many nuclear density distributions that fulfill the conditions set by the constraints and the Hartree-Fock-Bogoliubov (HFB) equations. In the self-consistent procedure only one shape is selected and it is the one which fulfills the condition of locally minimal energy of the nucleus. This approach guarantees that the selected shape is optimal within the given set of constraints, although nonconstrained degrees of freedom are not fixed.

*anna.zdeb@cea.fr
†michal.warda@umcs.pl
‡luis.robledo@uam.es

In consequence, in this method, the problem of too small deformation space (too few deformation parameters) does not exist. Nevertheless, the results provided with this method are not always unique [25] as one can easily land for a given set of constraints in one of the local minima. As a consequence, the self-consistent minimization procedure can produce several solutions with the same value of the constraints but different energies depending, for instance, on the starting wave function used in the solution of the variational equations. Those "multivalued" solutions are connected in a higher dimensional deformation space by a barrier separating them. A typical example, often seen in axially symmetric calculation constraining in the quadrupole moment, is the existence of two solutions with the same quadrupole moment but different values of the octupole moment in the region of the second barrier. The two coexisting minima are linked by a path going through the octupole moment in the parameter space. One of the unwanted consequences of this kind of situation is the possibility to jump between configurations when considering the behavior of quantities as a function of the current shape parameter. The leap is unphysical because one is skipping the path connecting the coexisting minima. When describing this situation, one talks about jumping from one fission valley to another. Whether the dynamics of fission justify this transition or it is just an artifact due to the limited number of constraints used to describe the fission path is a delicate issue that will be the subject of the present paper.

When several different solutions exist as local minima of the potential energy for a given set of constraints, one has to decide which of them should be considered in the analysis of fission. We may even encounter situations where, on the edge between two valleys, a *fake* or *missing* saddle can be found [25]. The first case occurs when two distinct nuclear shape configurations have the same energy at some coordinate, and the fission paths are incorrectly linked together. The missing one means that minimizing the energy with a single constraint may pass over a saddle leading to another valley. The consequence of a wrong interpretation of the PES may have a non-negligible impact on the description of fission dynamics. The barrier heights may be improperly evaluated, and some fission valleys may be omitted or redundant.

It has been previously shown that nongeometrical constraints like the one associated with pairing correlations may strongly influence the fission dynamics scenario because of the strong dependence of the collective inertias on the inverse of the pairing gap [26–31]. As a consequence, the inclusion of the pairing degree of freedom can substantially modify the dynamical evolution of a collective wave packet. Moreover, this kind of constraint can play a central role if the least action principle is used instead of the least energy one to determine the fission path. The treatment of spontaneous fission using the least action principle and including the pairing degree of freedom leads to a substantial reduction of the spontaneous fission lifetime [28–31]. However, and despite its relevance, we are not considering the pairing degree of freedom in the present study.

This paper is devoted to the discussion of the choice of the multipole moments to be used as constraints for the calculation of the PES leading to fission in the self-consistent methods. The primary purpose is to determine which subspace of collective coordinates in a deformation space is sufficient for an accurate description of static properties of fissioning nuclei. We will analyze the mechanism leading to multiple solutions of the HFB equations with the same values of the constraints defining the deformation space. The consequences of this behavior will be discussed. We will indicate regions where the discontinuity of the PES may be found.

To carry out our investigation, we have chosen two isotopes representing two different fission modes: asymmetric (^{252}Cf) [32–34] and bimodal (^{258}No) [35,36]. With this choice, we cover a broad and representative range of fission modes in heavy nuclei. The total half-life of the radioactive isotope ^{252}Cf is $t_{1/2} = 2.645(8)$ yr with alpha decay as the dominant branch. Only 3.092(8)% of the decaying nuclides undergo spontaneous fission. On the other hand, ^{258}No has a far shorter half-life $t_{1/2} = 1.2(2)$ ms and fission is the principal decay channel [37].

II. THEORETICAL FRAMEWORK

The present study has been carried out using the self-consistent constrained Hartree-Fock-Bogoliubov (HFB) method with the finite-range density-dependent nucleon-nucleon Gogny interaction. We use the D1S parametrization [38] that has been extensively used in the literature to describe many different nuclear structure phenomena [39,40] including the microscopic description of fission [41–45]. The latter is not surprising as the D1S parametrization was fitted to the fission barrier of ^{240}Pu in order to correct for a too large surface energy of the D1 Gogny force. On the other hand, D1S is not specially good at binding energies, showing an unphysical drifting with neutron number for this quantity [46]. To remedy this situation the parametrization D1M was proposed in Ref. [47]. As D1M's surface energy properties are, by construction, very similar to those of D1S it should not be surprising that potential-energy surfaces for fission are very similar with the two parametrizations [16,23].

In the HFB method [2,40], the nuclear states are obtained as the solutions of the HFB equations, which are derived by requiring that the mean value of the Routhian is a minimum:

$$\delta\left(\langle\Phi|\widehat{H} - \lambda_Z\widehat{Z} - \lambda_N\widehat{N} - \sum_{ij}\lambda_{ij}\widehat{Q}_{ij}|\Phi\rangle\right) = 0. \quad (1)$$

Here $\widehat{H}$ is the microscopic Hamiltonian, λ_N and λ_Z are the Lagrange multipliers used to fix the number of neutrons N and protons Z, while λ_{ij} are the Lagrange multipliers associated with the average value of the multipole moments $\widehat{Q}_{ij}$ with multipolarity i and projection j. In this work the quadrupole (Q_{20}), octupole (Q_{30}), hexadecapole (Q_{40}), and triaxial quadrupole (Q_{22}) deformation parameters are considered. The equations are solved by expanding the creation and annihilation quasiparticle operators of the Bogoliubov transformation in a harmonic oscillator basis with oscillator length parameters optimized for each set of collective deformation parameters to minimize the binding energy. Most of the results are obtained in the axial regime with an axially symmetric deformed oscillator basis with $N_\perp = 15$ and $N_z = 22$. This

basis is well suited to describe elongated shapes along the z axis such as those typical of fission. Beyond-mean-field two-body kinetic energy correction and rotational energy correction are included in the calculation of the binding energy. In the calculations with nonzero triaxial multipole moment Q_{22} reflection symmetry is preserved, and therefore odd multipole moments are zero by construction and not considered in the discussion. For the "triaxial" calculations an oscillator basis containing $N = 18$ shells is used.

The multipole moment operators are defined as

$$\hat{Q}_{lm} = \frac{1}{\sqrt{2(1 + \delta_{m0})}}(\hat{M}_{lm} + r_m(-1)^m\hat{M}_{l-m}) \qquad (2)$$

with $r_m = 1$ if $m \geqslant 0$ and -1 if $m < 0$. The raw multipole operators $\hat{M}_{lm}$ are given by

$$\hat{M}_{lm} = \sqrt{\frac{4\pi}{2l + 1}}r^l Y_{lm}(\theta, \varphi)$$

$$= \sqrt{\frac{(l - m)!}{(l + m)!}}r^l P_{lm}[\cos(\theta)]e^{im\phi}, \qquad (3)$$

where Y_{lm} are spherical harmonics and P_{lm} are associated Legendre polynomials. Using the standard definition of the spherical harmonics we obtain $\hat{Q}_{20} = z^2 - \frac{1}{2}(x^2 + y^2)$, $\hat{Q}_{30} = z^3 - \frac{3}{2}(x^2 + y^2)z$, $\hat{Q}_{40} = z^4 - 3(x^2 + y^2)z^2 + \frac{3}{8}(x^2 + y^2)^2$, and $\hat{Q}_{22} = \sqrt{3}/2(x^2 - y^2)$.

The computations were performed using the self-consistent HFB solver HFBAXIAL that uses the approximate second-order gradient method [48] to solve the HFB equations and the formulas of [49] for an accurate evaluation of the matrix elements of the Gaussian central potential for the large basis required in fission. The program starts from an initial wave function and iteratively minimizes the energy subject to a given set of constraints. In this procedure, the shape of the nucleus is adjusted to fulfill the conditions imposed by the constraint parameters.

As the initial configuration is expected to be "close" to the sought solution, this choice represents a way to decrease the number of iterations required in the minimization process and, therefore, represents substantial computer time savings. The final solution may depend on the starting point in specific cases. This feature will be thoroughly discussed below. Usually, the initial configuration is taken from a neighboring, previously computed wave function. In most of the cases we select the starting configuration from the nearest point with smaller quadrupole or octupole moment and eventually larger hexadecapole moment. Sometimes, when it is indicated, we take the starting configuration from the opposite side. In most of the cases the choice of the initial configuration is irrelevant for the final result. Only in special cases discussed in Sec. III does it affect the results obtained. As mentioned in the Introduction, the use of a limited set of constraints always introduces some uncertainties in which wave functions belong to the neighborhood of which local minima. To help in the characterization of the different solutions of the HFB equations it is convenient to use a technique based on searching for sharp changes in the matter density distribution all over the PES. The so-called *density distance* $D_{\rho\rho'}$ [25] has been used
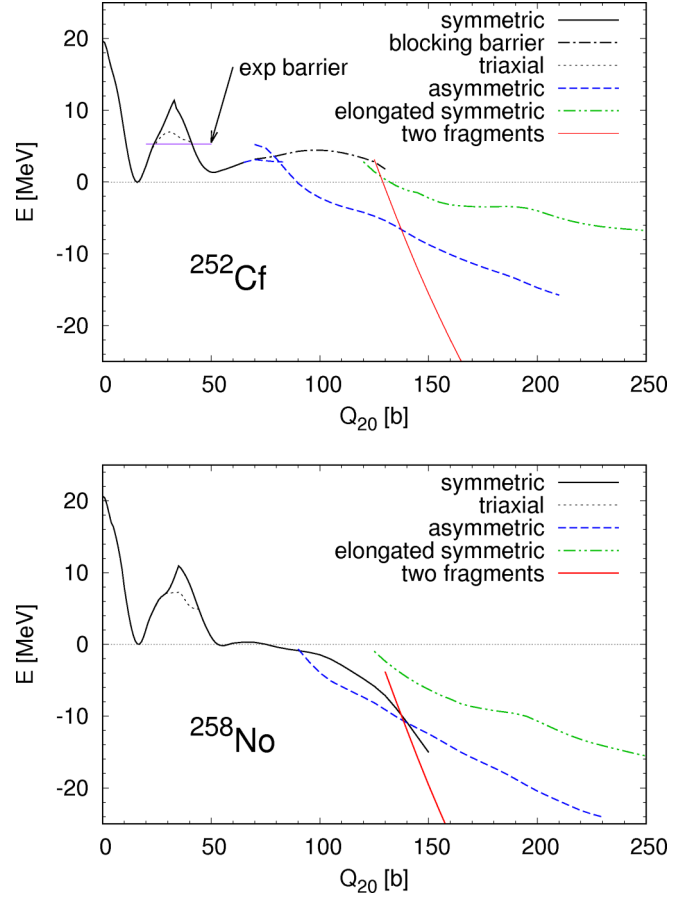

FIG. 1. Various fission paths for ^{252}Cf (top) and ^{258}No (bottom) are plotted as a function of Q_{20}. See text for details.

to detect such discontinuities in calculations considering the pairs of shape parameters Q_{20}-Q_{30} as well as Q_{30}-Q_{40}. For given configurations with matter density distributions $\rho(\mathbf{r})$ and $\rho'(\mathbf{r})$, the density distance is defined as

$$D_{\rho\rho'} = \int |\rho(\mathbf{r}) - \rho'(\mathbf{r})|d\mathbf{r}. \qquad (4)$$

Density distance remains small when nuclear shapes are similar, and it increases wherever there is a substantial change of nuclear shape for the two densities considered.

III. RESULTS

A. The PES in many coordinates

The theoretical description of fission is based on the analysis of the topography of the PES when represented as a function of the deformation parameters related to the elongation of the nucleus. More elaborate studies also include parameters related to reflection asymmetric shapes as they are required for the description of the asymmetry in fission fragment mass distribution. The inclusion of several shape parameters is also helpful in better characterizing not only
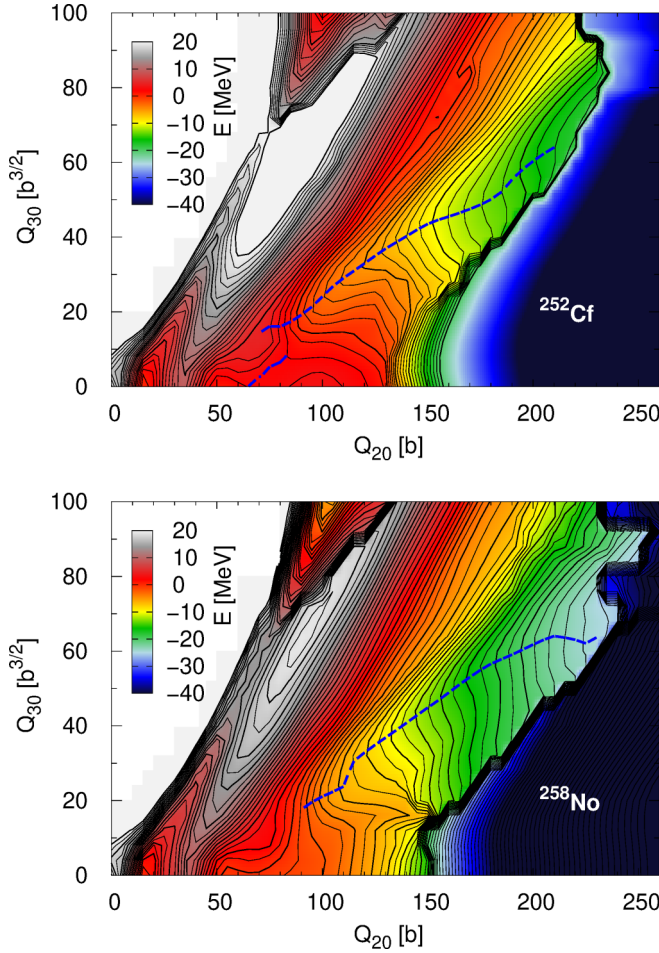
FIG. 2. The PES of ^{252}Cf (top) and ^{258}No (bottom) as a function of Q_{20} and Q_{30} are shown as contour and color plots. Constant energy contours are plotted every 1 MeV. The asymmetric fission path is represented by a blue dashed line.

FIG. 3. The PESs in the Q_{20}-Q_{22} plane for ^{252}Cf (top) and ^{258}No (bottom) are shown as contour and color plots. The isoenergy contour lines are plotted every 1 MeV. The dashed line shows the fragment of the fission path around the first barrier with nonzero triaxial deformation.

the height but also the shape of the fission barrier.[1] The shape of the fission PESs of ^{252}Cf and ^{258}No are shown in Fig. 1 as a function of the quadrupole deformation. In Fig. 2, the PES maps in the quadrupole-octupole plane are displayed for the same isotopes. The mesh points used to obtain the maps are calculated every $\Delta Q_{20} = 5$ b and $\Delta Q_{30} = 4$ b$^{3/2}$.

The results presented in Fig. 2 have been calculated in the axial regime. However, nonaxial shapes are crucial to describe the region of the first fission barrier correctly, and therefore we present the influence of triaxial deformations on the PES in Fig. 3. To simplify the calculation, reflection symmetry is preserved in these triaxial calculations, and therefore all the shapes have zero octupole moment. Usually, it is assumed that the information obtained from the aforementioned one- and two-dimensional plots together with the collective inertia is

sufficient to describe the details of the fission process from the ground state till scission. Of course, they contain the key elements of the fission process like fission barrier heights, widths and fragment mass asymmetry. Nevertheless, there are several limitations to this approach. First, the collective motion explores not only the minimum energy path (or the minimum action path) but also its neighborhood due to the inherent quantum nature of the dynamics. There is a finite probability that the collective wave packet representing the evolution of the system towards fission explores regions close to the classical trajectory [50–52]. This exploration of neighboring configurations is also a feature of classical models used to mimic [53] the quantum mechanical evolution typical of the fission phenomenon. In this respect, the width of the valley, or, in other words, the stiffness of the potential energy, affects the spread of the collective wave packet and therefore the fragment mass distribution. Departure from the classical least energy fission path implies considering a broader set of nuclear shapes like those obtained by modifying the neck width and length or the shape of the prefragments. These variations

---

[1]Please note that the tunneling probability through the fission barrier depends exponentially on the square root of its height times its width, when approximated by a square potential barrier.
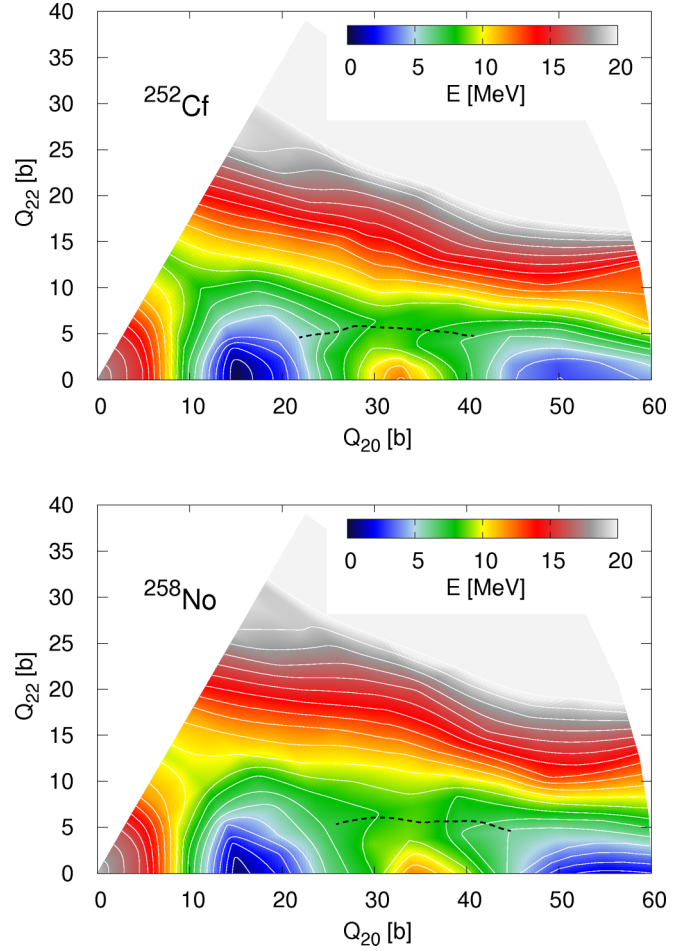
can lead to a change of the obtained mass asymmetry at the scission point. Special care should be taken on a possible reduction of the neck thickness, as it determines the scission configuration.

Another problem is that points on the Q_{20}-Q_{30} map are defined as local minima of the energy with given constraints on quadrupole and octupole moments. There is no guarantee that the minimum is unique. In fact, it was shown that sometimes there might exist multiple local minima in the energy that create different fission valleys in the same region of the Q_{20}-Q_{30} map [54], and the tunneling probability connecting them should be considered. On the other hand, if no explicit quantum dynamical treatment is carried out and the analysis is just restricted to exploring the PES, then, in order to predict fission observables, one has to decide which of the paths should be taken under consideration. Finding a consistent criterion to take a physically correct decision is not straightforward and, in some cases, it can be very difficult.

Thus, we observe that other degrees of freedom may affect some aspects of the theoretical description of fission. It is even the case when a two-dimensional map in the self-consistent calculations is created from nuclear shapes optimized in the procedure of energy minimization, not just created by a two-parameter formula. To better describe and understand fission, one has to increase the size of the considered space of constraints on which the PES is spanned and look at it from a broader perspective. In this way, one should be able to compare all the available valleys and deduce which path should be preferred by the evolving system.

In order to extend the space of deformation, the most natural and most often used coordinate is the next term in the multipole expansion: the hexadecapole moment Q_{40}, responsible for necking [54]. By decreasing the value of the hexadecapole moment, shapes with a thinner neck are obtained. The alternative option is applying the constraint on the neck parameter Q_N [42,55]. It produces the same effect as the hexadecapole moment, but it is more sensitive at the scission region and less precise elsewhere.

To visualize a three-dimensional PES is a difficult task that can somehow be facilitated if one of the variables is kept fixed and the PES for the remaining two variables is plotted as a contour plot. Such a procedure has been followed in Fig. 4 for ^{252}Cf and Fig. 5 for ^{258}No, where we show sections of the PES for fixed values of Q_{20} as maps in the Q_{30}-Q_{40} space. The black, blue, and red dots correspond to the least-energy fission paths found on the PES spanned on the Q_{20}-Q_{30} space. The black dots correspond to the lowest-energy minimum, the blue ones stand for the next-in-energy local minimum, and the red dots indicate the post-scission minimum corresponding to the two-fragment solution. The blue dashed lines show the results of two-dimensional calculations, where the hexadecapole moment is self-consistently given by the minimization of the total HFB energy with double constraints on Q_{20} and Q_{30}. The thick black line represents scission configurations and will be discussed below.

The analysis of the fission barrier in the next subsections will be based on all the above mentioned plots of the PES.

B. Detailed description of the PES

The fission barriers and the PESs obtained for the two nuclei considered agree with the expectations for nuclei in the heavy-actinides region. Both isotopes are prolate in their ground states with $Q_{20} = 16$ b. On the quadrupole-octupole map of the PES, one can see a fission valley heading towards large octupole deformation starting at the ground state. It describes superasymmetric fission strongly related to cluster radioactivity [56,57]. The minimum of the energy corresponding to this valley can be seen in Figs. 4 and 5 at $Q_{20} = 30$, 40, and 50 b and large octupole moments. The saddle point in the super-asymmetric valley reaches over 20 MeV and, in heavy actinides, leads to an exotic decay mode [57], not observed experimentally. We will not discuss this type of fission here.

The first reflection-symmetric barrier is located at around $Q_{20} = 30$–35 b. It is well known that triaxial deformation reduces its height [7,20,43]. In Figs. 1 and 3 we can see that the barrier width stays unchanged by including triaxiality but the sharp-peaked summit of the axial barrier is cut off by 4.7 MeV in ^{252}Cf and 3.7 MeV in ^{258}No. The fission barriers including triaxiallity are 7.0 and 7.3 MeV high, respectively. The experimental value for ^{252}Cf is 5.3 MeV [58,59]. Triaxial deformation of the fission path is relatively small, $\gamma \leqslant 12°$. At around $Q_{20} = 50$ b the nucleus goes back to fission through axial shapes, and triaxiality is negligible for larger elongations.

The modification of the landscape by including triaxial deformations is non-negligible, but its influence on the spontaneous fission half-life depends on the value of the collective inertia along the triaxial path as compared to the axial one. There are indications that triaxiality should not affect fission dynamics since the energy decrement at the saddle is compensated in the calculation of the collective action by the increase of the collective inertia and, therefore, the tunneling probability is larger along the axial path [43,60]. Please note that despite the similarity in barrier heights, the experimental fission half-lives of the two isotopes differ by 12 orders of magnitude [61]. The key to understanding this result, implying quite different barrier penetrabilities, is the existence of a second barrier in ^{252}Cf that disappears in the ^{258}No case, reducing the effective width of the total barrier dramatically. In consequence, theoretical fission half-lives are $\log_{10}(t_{1/2}/s) = 8.74$ for ^{252}Cf and $\log_{10}(t_{1/2}/s) = -1.94$ for ^{258}No (calculated in the axial regime). These values are less than one order of magnitude away from experimental data.

The second minimum can be found at an energy as low as 1.3 MeV above the ground state at $Q_{20} = 50$ b in ^{252}Cf and 0.2 MeV below the ground state at $Q_{20} = 55$ b in ^{258}No. In both isotopes, the shapes of the nucleus are axially and reflection symmetric in the second minimum. A well pronounced fission valley with nonzero octupole deformation opens up at larger elongation in both isotopes. The topography of the PES beyond this point is crucial for determining the fission fragments' mass asymmetry and fission half-lives. The key factor is whether the nucleus would prefer to stay in the symmetric fission path or rather turn into the octupole valley. The main distinction between ^{252}Cf and ^{258}No can be found in the shape of the symmetric fission barrier and the shape
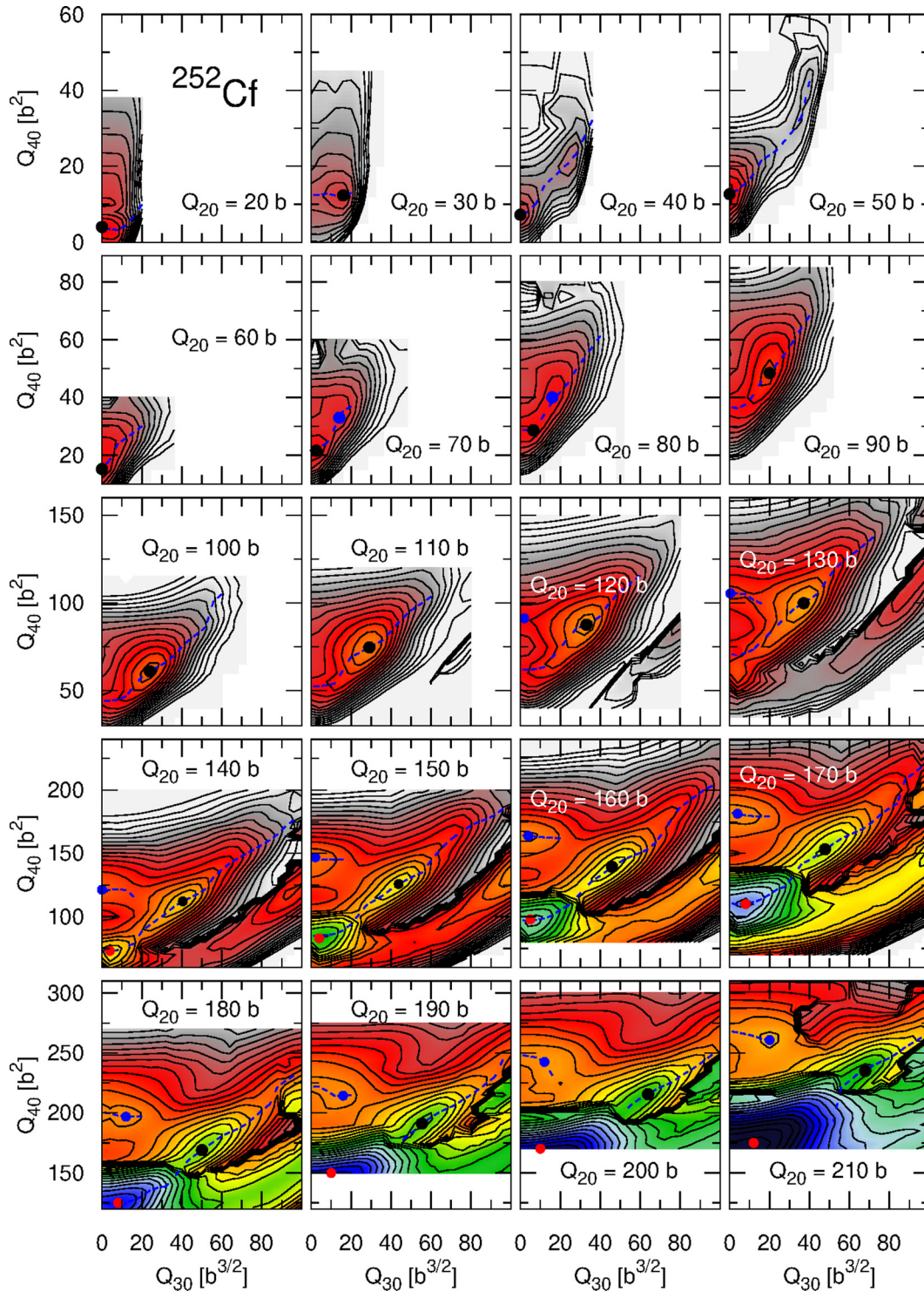
FIG. 4. The PES of ^{252}Cf in the Q_{30}-Q_{40} plane is shown as a contour and color plot. Constant energy contours are plotted every 2 MeV. The energy color scale is the same as in Fig. 2. See text for details.

of the energy surface around $Q_{20} = 100$ b for small octupole deformation. The difference is relatively small in absolute values but provides important consequences for the fission properties.

One can notice in the ^{252}Cf PES that around deformation $(Q_{20}, Q_{30}) = (100$ b, 0 b$^{3/2})$ a 4.5-MeV high second barrier arises, which blocks the symmetric fission channel in this

isotope. In fact, from $Q_{20} = 70$ b, there is no local symmetric minimum on the PES (there is a peak, not a saddle in the two-dimensional plot), and hence the barrier is plotted with a dash-dotted line in Fig 1. In this region, remaining at zero octupole moment is energetically unfavorable as the potential energy grows 3.2 MeV above the second minimum and the asymmetric valley is easily reachable with small energy costs.
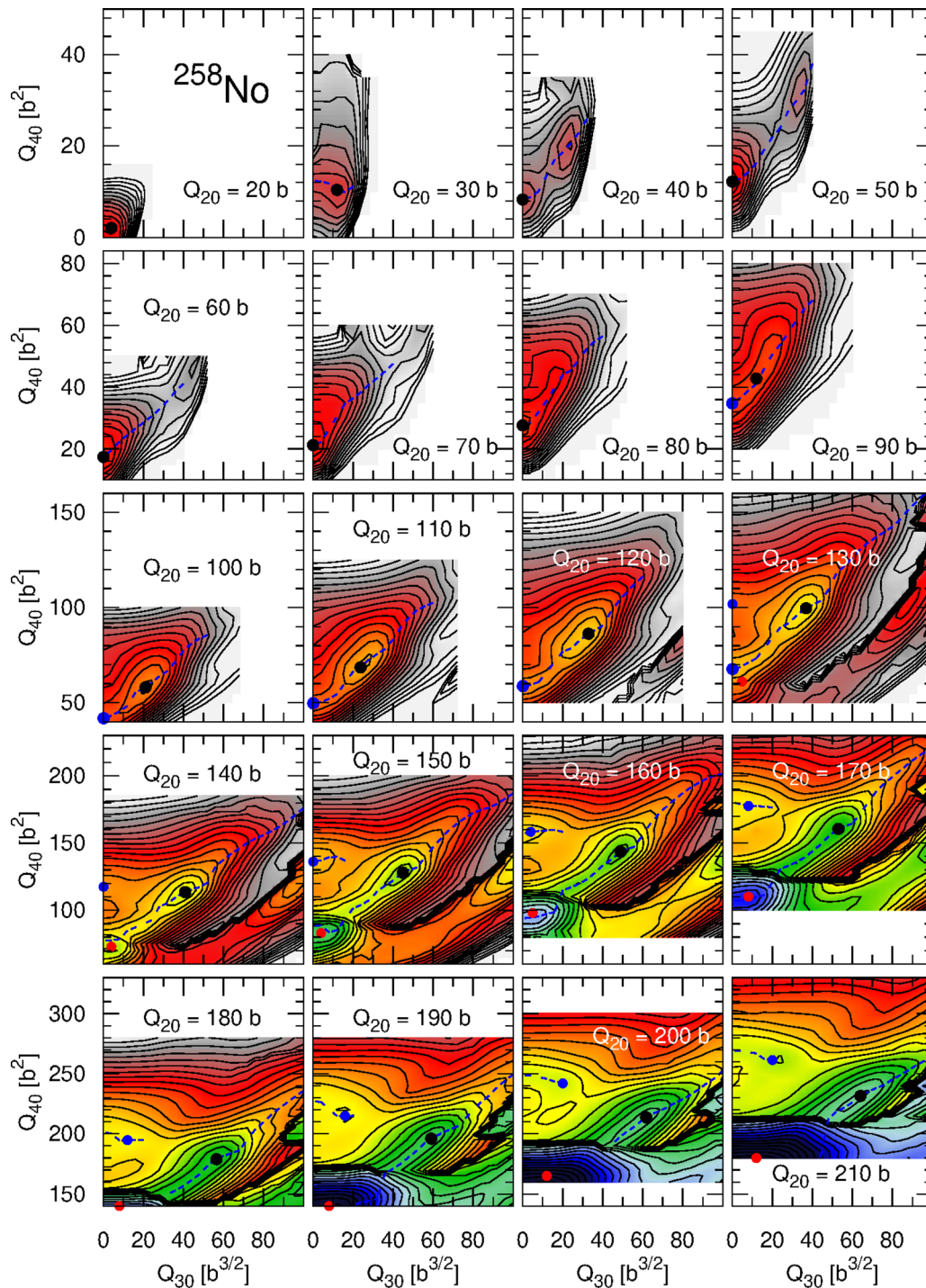
FIG. 5. The same as in Fig. 4 but for ^{258}No.

We can see in Figs. 1 and 4 that the asymmetric valley starts already at $Q_{20} = 70$ b and the second saddle is at 3.1 MeV above the ground state (1.8 MeV above the second minimum). Moreover, the energy in the asymmetric fission path rapidly decreases, reducing the barrier width.

In contrast, the second barrier in ^{258}No, located at $Q_{20} = 65$ b, is flat with a height which is only 0.7 MeV above the second minimum (0.3 MeV above the ground state). It is almost completely hidden below the ground state and therefore does

not contribute in a substantial way to the half-life, as mentioned above. At $Q_{20} = 90$ b the asymmetric valley opens up without any additional barrier (see Fig. 5). The fission process may proceed in the asymmetric mode, but the nucleus may as well stay at the reflection symmetric path without energetic costs. This fact explains the experimentally observed bimodal fission mass distribution with a small (5% abundance) component with high kinetic energy and mass symmetric distribution [35,36].
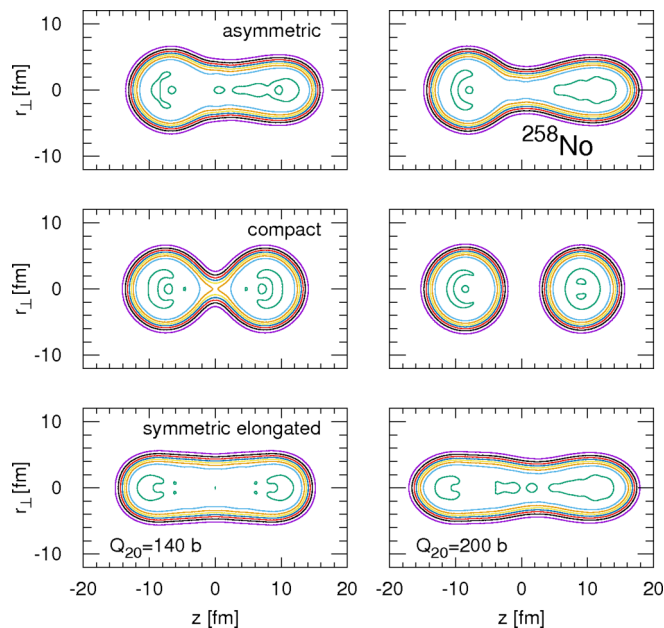
FIG. 6. The density distribution of ^{258}No at $Q_{20} = 140$ b (left) and $Q_{20} = 200$ b (right) in various fission paths: asymmetric (top), compact before and after scission (middle), and elongated symmetric (bottom).

The topography of the Q_{30}-Q_{40} planes given for fixed quadrupole moment and shown in Figs. 4 and 5 has quite a simple structure up to the region of the second barrier. We can see only one—or at most two—local minima in parabolic-shaped valleys. In the final phase of the fission process, the PES is far much complex. Already at $Q_{20} = 120$ b in both isotopes we can see several branches of the fission valley with two or three local minima for the same quadrupole moment. The first one is octupole deformed. Its shape is depicted in the top panel of Fig. 6. It leads to an asymmetric fission-fragment mass distribution, and therefore we refer to it as an *asymmetric* mode. The second one with $Q_{30} = 0$ b$^{3/2}$ and small values of Q_{40} (around 50–70 b^2) is a natural continuation of the symmetric fission path. The nuclear shape consists here of two almost spherical prefragments; see the middle panel of Fig. 6. This one is often called a *compact* mode of fission. By stretching this configuration, we increase the distance between prefragments and make the neck thinner up to its disappearance. The compact path is continued after scission with two separated fragments. For a two-fragment solution, further increase of the quadrupole moment leads to an increase of the distance between daughter nuclei instead of a shape change. The minimum of the energy is obtained for a configuration with a small mass asymmetry between fragments and, in consequence, a small octupole deformation.

The third minimum also corresponds to reflection symmetric shapes, but the hexadecapole moment takes much larger values, over 90 b^2. In this configuration, pre-fragments are not well disentangled. The shape is almost cylindrical: *cucumber-like* with a small reduction of thickness in the region of the neck (bottom panel of Fig. 6). This solution is called *symmetric elongated* mode [62,63]. Small reflection asymmetry can

also be found here, especially for large quadrupole moments. The corresponding fission path is the highest in energy, and it survives up to a very large elongation of the nucleus as the neck is not formed and a rupture of the system is not possible without a substantial energy cost. Calculations with the Skyrme energy density functional suggest that this fission path is energetically comparable with an asymmetric path around the second barrier in the nuclei from the region of heavy actinides and may play an important role in fission [62,63].

We should stress here that the crossing of fission paths in Fig. 1 cannot be interpreted as a possible place of bifurcation or configuration change. This is a typical example of a fake saddle point [25]. The fact that two or even three lines have the same energy for the same quadrupole moment does not mean that they represent the same or similar shapes of the nucleus. As one can see in Fig. 6 the differences in the nuclear density distribution between fission paths are usually huge.

The existence of two local minima and surrounding local valleys (e.g., compact and symmetric elongated) at the same quadrupole and octupole deformation leads straight to the multiplication of the surfaces on the traditional elongation–mass asymmetry maps, as in Fig. 2. The blue dashed lines in Figs. 4 and 5 indicate solutions corresponding to the local minimum of the energy for fixed Q_{20} and Q_{30}, i.e., these data could be used to create the PES map in the (Q_{20}, Q_{30}) space. Mixing values coming from different valleys may lead to an ambiguous and often erroneous interpretation of the calculated results which might eventually suggest contradictory conclusions. As the surfaces are often similar in energy, the choice of the surface would likely be a matter of a random selection by a numerical procedure or an arbitrary decision of the researcher. There is also the risk of an accidental change of the surface. This effect could easily be missed in the analysis of fission as graphical plotting programs are likely to smooth out sharp ridges. The application of the density distance parameter described below in Sec. III C can be useful to prevent these nonphysical interpretations.

In the analysis of Figs. 4 and 5 various scenarios for reaching pre-scission configuration can be envisaged. The scission line is visible in these plots for $Q_{20} \geqslant 120$ b as a black line (consequence of plotting many closed energy contour lines) separating single shapes (above) from two-fragments configuration (below). The rapid change in the energy is a consequence of the strong dependence of the neck on multipole moment parameters: slight changes lead to a strong reduction of the neck and eventually to the splitting of the nucleus (see discussion below).

Beyond the region of the second fission barrier ($Q_{20} = 100$ b), the PES goes down towards scission. The pre-scission line, i.e., the line of the most elongated shapes before the rupture of the neck, is clearly seen at Fig. 2 as a few-MeV-high cliff that separates the fission valley from the two-fragments configuration. There are several ways of reaching a scission configuration: The first is through a symmetric compact mode. Increasing elongation leads to a relatively smooth shape evolution from pre- to post-scission configuration. Nevertheless, even if an energy fall is not noticed, an abrupt change in the nuclear density distribution around the neck region is

visible (e.g., see [64] for the ^{258}Fm case). The two dimensional Q_{30}-Q_{40} sections of the PES between $Q_{20} = 120$ and 130 b in ^{252}Cf and between 150 to 160 b in ^{258}No do not differ substantially despite a few MeV energy drop in the minimum of the valley. It indicates that the pre- and post-scission density distributions of the whole system are relatively similar despite the neck rupture. Another, mostly intuitive way of reaching a scission point from the asymmetric fission valley is by going along the fission path (marked with the blue dashed line in Figs. 1 and 2 and black dots in Figs. 4 and 5) to the largest possible quadrupole moment. As the energy decreases simultaneously with increasing elongation, the largest gradient indicates that this is the most probable fission scenario. The large mass asymmetry $A_H/A_L \approx 140$–$142/112$–116 obtained before the neck rupture in this point corresponds to the experimentally observed most probable fission fragment asymmetry.

The two scenarios presented above for the evolution of the nuclear shape assume that the system remains on the fission paths presented in Fig. 1. Therefore, only one or two particular shapes of the nucleus are taken at scission. Such analysis can explain the fission modes observed in the experiment, but it is insufficient to reproduce the details of the fission fragment mass distribution. The reason is that, on its way from the saddle to scission, the collective wave packet may explore different configurations away from the lowest energy fission path, still fulfilling the condition of descending energy but not with the largest gradient. In this way, every configuration of the scission line in the neighborhood of the asymmetric fission valleys which are visible in Fig. 2 is accessible, of course with a reduced probability [51]. These configurations can be observed in Figs. 4 and 5. For $Q_{20} \geqslant 140$ b the post-scission compact minimum in the lower right corner of each panel has lower energy than on the asymmetric path. The latter valley seems to be soft in the direction towards the first one, and the ridge separating them does not exceed 2 MeV. Those figures indicate that the exit points from the asymmetric fission valley are available already at relatively small octupole moments and with a smaller asymmetry of nuclear shapes than at the end of the asymmetric fission path.

Two additional aspects of this scenario must be pointed out. First, a scission point is accessible already for a much less elongated configuration than at the end of the asymmetric fission path. In some lighter nuclei, where a scission point is above the ground state energy, this would reduce the width of the barrier. In consequence, tunneling probability increases and the half-lives can be substantially shortened [54]. Second, at smaller quadrupole moment, the asymmetric valley at low octupole moment ends up not in fusion valley but in the compact fission valley before scission. This is another mechanism of feeding the symmetric mode of fission. Thus, the dynamical calculations of the fission mass yields for ^{252}Cf, where only quadrupole and octupole deformations were taken under consideration, showed a small contribution for the symmetric mass division [51].

C. Surface discontinuity and density distance

As mentioned in Sec. II, the density distance is an appropriate quantity to test the continuity of the PES. This issue is
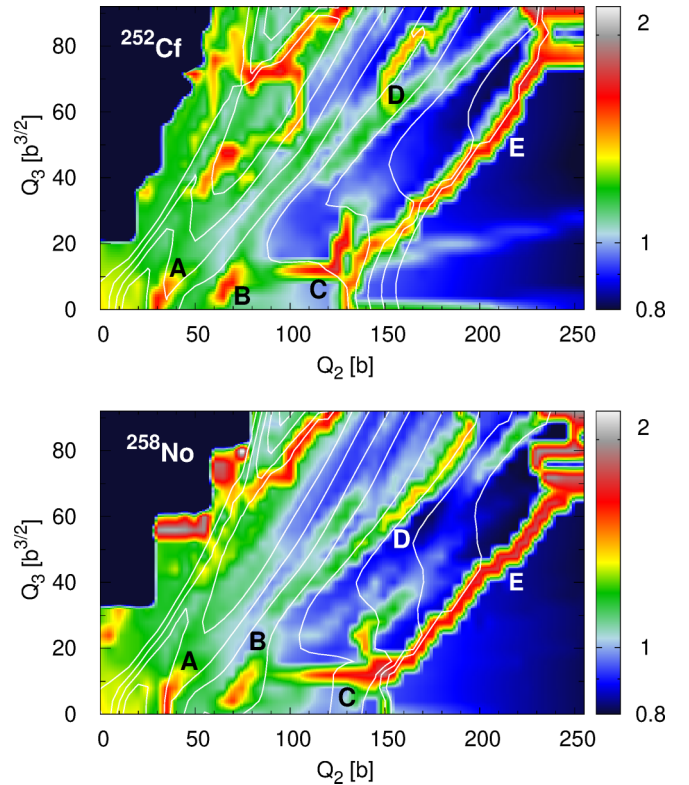

FIG. 7. The density distance function $D_{\rho\rho'}$ (in logarithmic scale) given by Eq. (4) between two neighboring configurations in a deformation space Q_{20}-Q_{30} of ^{252}Cf (top) and ^{258}No (bottom). Contour lines for the energy are plotted every 5 MeV for better identification of the different regions of the PES.

very important as one may draw false conclusions concerning fission dynamics. In Fig. 7 we have plotted, for each point in the (Q_{20}, Q_{30}) plane, the largest of the two density distances computed for the two configurations $(Q_{20} + \Delta Q_{20}, Q_{30})$ and $(Q_{20}, Q_{30} + \Delta Q_{30})$. The figures look pretty similar for both isotopes and a few regions of large $D_{\rho\rho'}$ can be identified:

(1) first barrier;
(2) around the second minimum;
(3) between the symmetric and asymmetric valleys at $Q_{30} \approx 15$ b$^{3/2}$;
(4) bordering the asymmetric valley at large octupole deformation;
(5) scission line.

We will denote these regions as "regions of discontinuities" due to the large difference in densities corresponding to neighboring points indicating possible abrupt change of configuration.

The first region of discontinuity, A, is encountered already at the first barrier. The nucleus has a double cone (diamond) shape on the up-going part of the barrier, whereas a two-center structure is created beyond the maximum of the barrier, as can be seen in the left panels of Fig. 8. The two density distributions are clearly different, with a significant jump in hexadecapole moment. A sharp peak of the first fission barrier also indicates a sudden change of configuration, and the fake
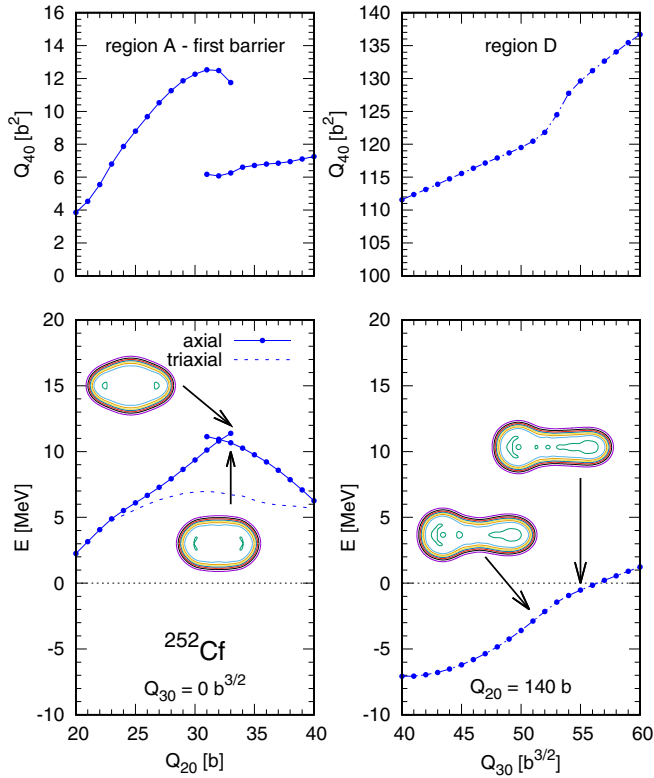
FIG. 8. Fragments of the first barrier and asymmetric valley at fixed $Q_{20} = 140$ b of ^{252}Cf.

or missing saddle mentioned above is usually present [25] because two solutions can be found for the same quadrupole moment around the peak. The density distance calculated in this region does not take into account the influence of triaxiality discussed in Sec. III A that eliminates discontinuities.

In the right panels of Fig. 8, the region D of enhanced density distance is observed. As we can see, there is no discontinuity here but only a change of the hexadecapole moment can be observed in this region. The source of this kink can be explained by looking at Figs. 4 and 5. The valleys plotted in the Q_{30}–Q_{40} planes around $Q_{20} = 140$ b lie along a more or less straight line with a slope of the order of 1. We determine the localization of the bottom of these valleys by minimization with a constraint on the octupole moment (marked by blue dashed lines). This procedure sometimes does not give the correct value that is obtained by following the direction of the gradient along Q_{30} and Q_{40} that determines the bottom of the valley. As a consequence of the improper determination of the bottom of the valley using a constraint on the octupole moment, large increases in the value of Q_{40} can be noticed between $Q_{30} = 50$ and 55 $b^{3/2}$ in Fig. 8. No real discontinuity of the surface is found here, but rather a problem with the precise numerical evaluation of the bottom of the valley and therefore no important physics is missed here.

The regions C and D should be discussed together as they separate the compact symmetric and the asymmetric fission valleys. A first look at the PES in Fig. 1 reveals a seemingly smooth surface: no sharp ridges or sudden energy changes. Therefore, it comes as a surprise to find a discontinuity here.

To solve this puzzle, one has to use a magnifying glass: in Figs. 9 and 10 we have plotted a blown-up view of the sections of both valleys in ^{252}Cf and ^{258}No, respectively. The step size in these calculations was reduced to $\Delta Q_{30} = 1$ $b^{3/2}$ with starting point from the nearest mesh point with smaller or larger octupole moment.

In the left columns of Figs. 9 and 10, the PES in the second minimum is plotted. In this case, the energy grows up smoothly with increasing mass asymmetry. Only a small bending in hexadecapole moment can be noticed. The PES picture at $Q_{20} = 70$ b, in the region B of discontinuity, is completely different; see panels in the second column. The PES consists here of two parts clearly distinct in hexadecapole moment. In the first part, for low octupole moments, the nucleus has a well-shaped neck and a small hexadecapole moment, below 30 b^2. Increasing octupole deformation above 10 $b^{3/2}$ causes a jump in hexadecapole moments which indicates the change of configuration and the neck is not pronounced anymore. This rearrangement is not followed by a change of the energy but only by a change of its slope with increasing octupole moment. It is easy to distinguish here the compact valley from the elongated asymmetric one. Moreover, in ^{252}Cf, the asymmetric valley can be extended towards lower octupole moments up to zero. This is the germ of the symmetric elongated fission valley. Discontinuity in the region B is not a significant problem in the description of fission as a transfer from the second minimum to the asymmetric valley requires a few additional MeV of energy, which practically blocks such evolution.

Increasing the quadrupole moment, we find a space between regions B and C in Fig. 7. Its impact is also visible in Figs. 9 and 10 at $Q_{20} = 90$ b. Here, the PES as a function of Q_{30} is continuous again. Hexadecapole moment gradually increases, indicating a smooth connection between the compact and asymmetric valleys. The transfer between configurations is possible as a consequence of decreasing the energy of the asymmetric minimum. The tiny part of the symmetric elongated surface can be noticed only very close to reflection symmetric shapes.

The rightmost panels of Figs. 9 and 10 describe the region C of discontinuity. Despite the same values of the quadrupole and octupole moments and the similarity of energies, the hexadecapole moments and the shapes of the nucleus are considerably distinct in both configurations. In the compact symmetric mode, two pre-fragments are separated by a thin neck. In the asymmetric mode, the density distribution is more uniform along the symmetry axis. In both isotopes, the compact mode is limited to hexadecapole moments in the range from $Q_{40} = 50$ to 60 b^2 whereas the asymmetric mode is described by much higher values, over 65 b^2. In ^{252}Cf, the compact valley created by increasing the octupole moment ends with a sudden drop into the asymmetric valley. In this nucleus, by decreasing octupole moment in the calculations of consecutive mesh points in the asymmetric valley, one may reach zero octupole moment in a configuration characteristic of the elongated symmetric valley. The transition from the compact to the asymmetric valley is an analog of the scission line discontinuity described below. In ^{258}No both surfaces meet at the same energy, and the elongated symmetric part
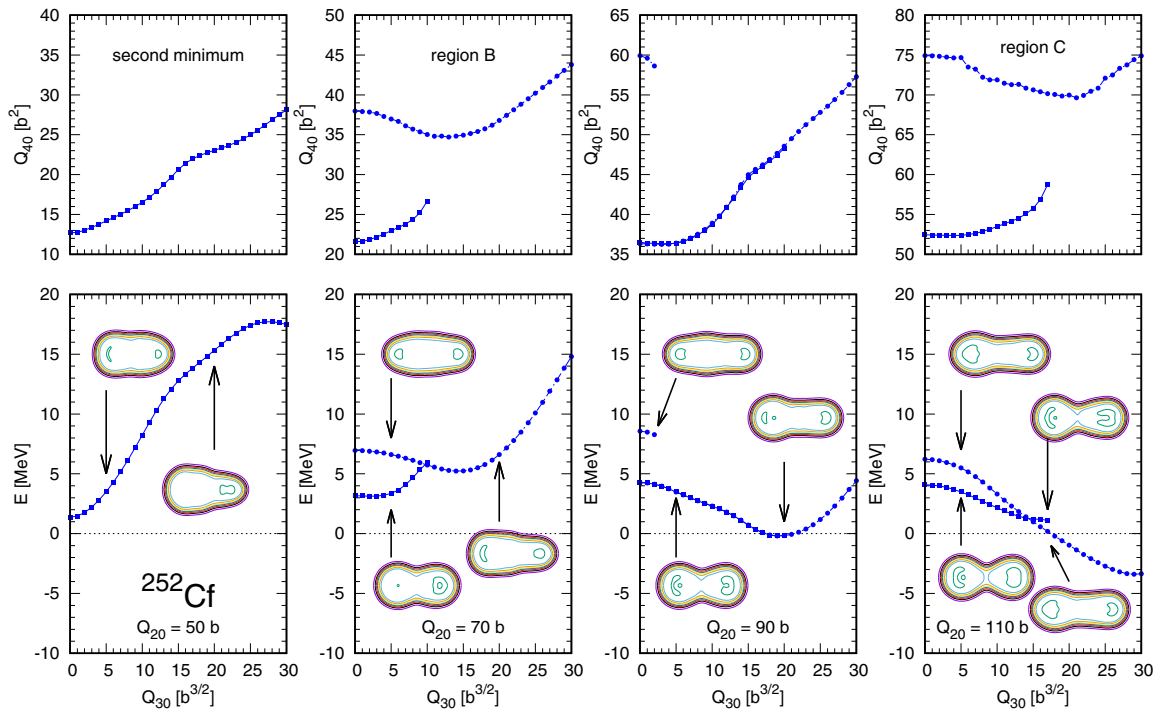
FIG. 9. Fragments of the PES of ^{252}Cf at fixed $Q_{20} = 50$, 70, 90, and 110 b.

cannot be determined at $Q_{20} = 110$ b. In region C, in both isotopes, transfer to the asymmetric valley is energetically favorable.

The transition between configurations in this region is usually overlooked. It is easy to incorrectly link the two valleys

when the distance between mesh points is as large as 4 or 5 $b^{3/2}$, which is usually a reasonable choice for producing the PES maps. The similarity of the energy slopes as well as the fact that increasing octupole moment on the compact valley beyond its end leads to a solution in the asymmetric one (by
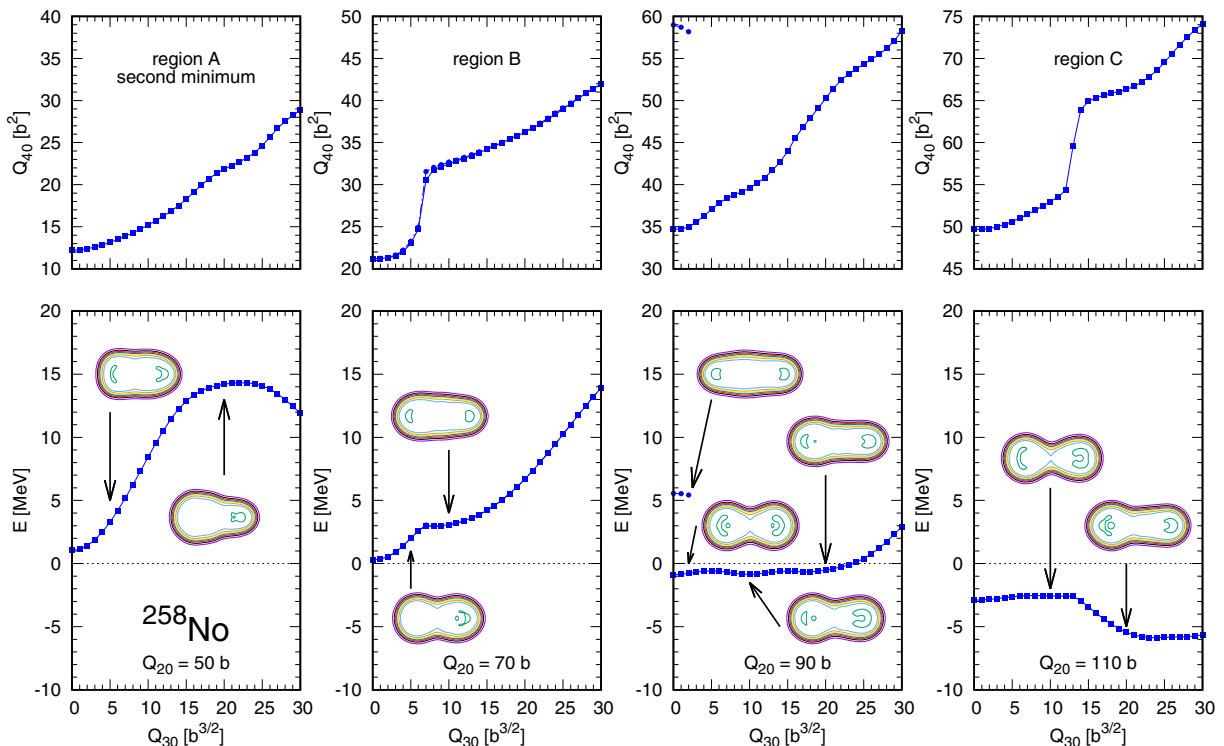

FIG. 10. The same as in Fig. 9, but for ^{258}No.

applying the self-consistent energy minimization) enhance the chances of making mistakes.

Looking at the energy section maps in Figs. 4 and 5 we find that the discontinuity between symmetric and asymmetric surfaces discussed above is a good example of missing saddles as discussed by Dubray and Regnier [25]. In a three-dimensional PES, the problem of a rapid change of configurations disappears.

Finally, a commonly known discontinuity is localized in the region E of the scission line. There is a huge difference in pre-scission and post-scission configurations. It is very hard or even impossible to find a continuous link by using constraints on multipole moments to control the nuclear shape. Applying constraints on the neck parameter Q_N may help to provide a continuous surface on the scission line [55,56].

Let us discuss now the source of the scission line *cliff* obtained in the self-consistent calculations. The asymmetric valley in two-dimensional space is made of configurations which are local minima along *all* the directions orthogonal to the ones of the constraints. In consequence, decreasing the neck thickness (or hexadecapole moment) leads to increasing the energy of the system even though the ruptured nucleus is energetically favorable. The height of the barrier separating the asymmetric path from the no-neck solution decreases to zero with increasing quadrupole moment. Beyond the pre-scission line, any shape of the nucleus is unstable against neck rupture, i.e., the energy monotonically decreases with decreasing neck thickness. The energy minimization procedure cannot find a stable solution with a neck. The gradient of the energy directs the system towards post-scission configuration with much lower energy in the self-consistent process. Of course, the cliff on the scission line does not mean that in nature the neck disappears instantly, but only that a further thinning of the neck should occur without increasing the elongation of the system.

The concept of density distance can also be applied to the PES given as a function of the octupole and hexadecapole moments for fixed Q_{20} values. An example of the results is presented in Fig. 11. Here again, the discontinuity at the scission line is clearly visible. The density distance is also enhanced in some other regions of the PES quite randomly scattered on the surface. Its values are relatively small in comparison to the scission line ones. The only characteristic region of larger density distance separates the elongated symmetric valley from the compact one.

D. Multiple solutions

We have already shown that the description of fission in terms of a one-dimensional or even a two-dimensional PES may lead to many misunderstandings. Two or more different configurations can be obtained in the same location of the PES in those cases. This problem has been observed while discussing the region between the compact symmetric and the asymmetric valleys. Similar issues can arise if one analyzes the so-called fusion channel with two separate fragments. Decreasing the quadrupole moment of the system in this region leads to approaching fragments which are much closer than what can be achieved in the scission configuration. In
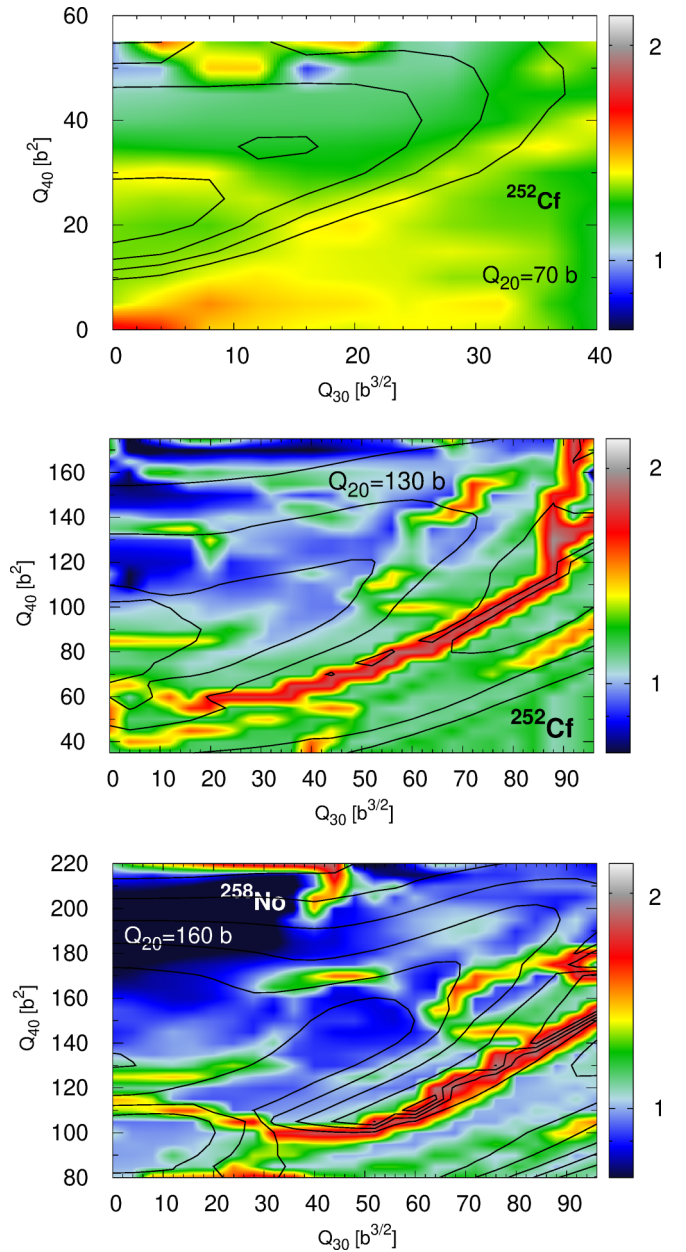

FIG. 11. The same as in Fig. 7, but for the PES at fixed Q_{20} in a deformation space Q_{30}-Q_{40} of ^{252}Cf at $Q_{20} = 70$ b (top) and at $Q_{20} = 130$ b (middle) and of ^{258}No at $Q_{20} = 160$ b (bottom). Contour lines of equal energy are plotted every 5 MeV for better identification of the different regions of the PES.

consequence, the fusion valley covers a much larger area than presented in Fig. 2. This surface, mostly "hidden" under the asymmetric fission valley from Fig. 2, is shown in Fig. 12. Only in the lowest quadrupole deformation region are the fragments close to each other, and Coulomb energy is so high that the fusion valley climbs up above the fission one. Since the global energy minimum for a given quadrupole moment may be in the post-scission configuration, an important physical problem appears. Should we take this solution as part of the PES leading to fission or rather stay in the fission valley as long as possible? The only way to tell is to do a dynamic
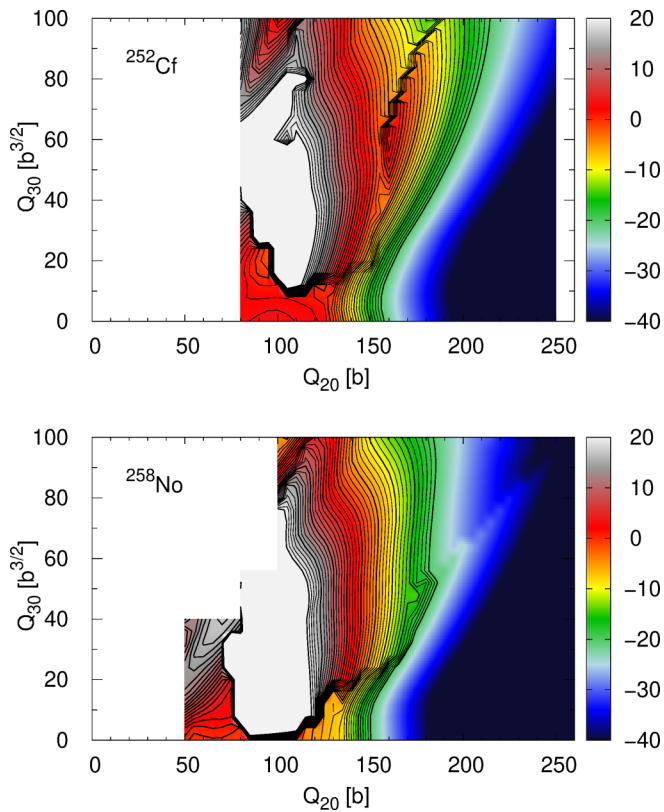
FIG. 12. The same as in Fig. 2 but the fusion valleys are plotted.

calculation, but if this is not available then the two possibilities and their consequences should be considered.

Two alternative approaches can be found in Fig. 1 of Ref. [65] by Regnier *et al.* and Fig. 1 of Ref. [64] by Warda *et al.* Both Figures show the PES of ^{258}Fm calculated with the same model and interaction (HFB theory and Gogny D1S force). Nevertheless, the shape of the asymmetric fission valley is different. In the first plot it is narrow and equipotential (the lines are mainly horizontal), whereas in the second case the asymmetric valley is wide and the lines of constant energy are rather vertical. The source of the difference comes from the distinct strategy of selecting the local minima for the surface. Regnier *et al.* selected the lowest of the local minima for the given constraints. Warda *et al.* paid more attention to the continuity of the changes in the shape and preservation of the valley in which a nucleus was located in the previous phase of evolution. In the first approach, the scission line is localized at a much lower elongation, and the PES includes a larger part of the fusion valley.

We would like to stress that, unexpectedly, both figures give the correct surface in two dimensions, showing the importance of considering multidimensional PESs. Restricting the deformation space to just one, two, or three dimensions simplifies the interpretation of the results as well as its graphical representation, but it can hide information, veiling our understanding of the nature of the fission process.

We would like to point out that one can observe an internal structure of the PES in the fusion channel. The surface is usually smooth, with mass and deformations of the fragments
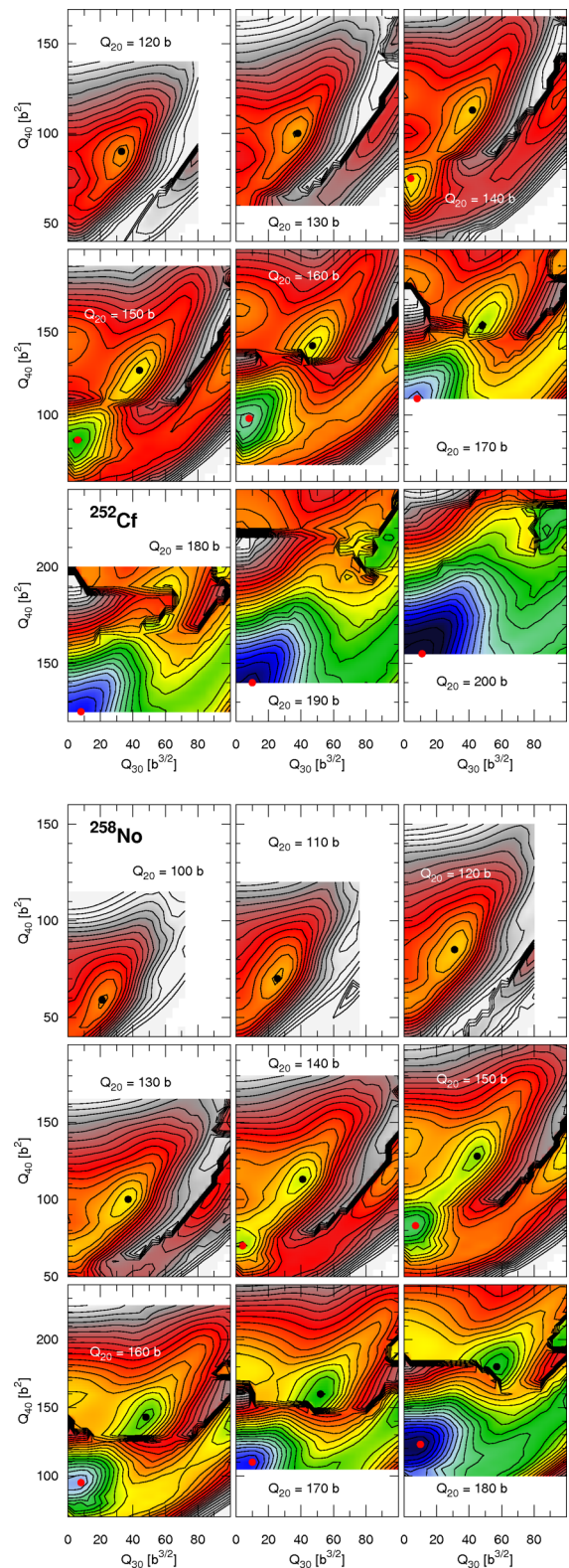

FIG. 13. The same as in Fig. 12 but for cross sections in the Q_{30}-Q_{40} plane. Black and red dots indicate localization of the fission and fusion paths, respectively.

gradually evolving with octupole moment. A rapid drop in the energy indicates an abrupt change of the fragment configuration.

The extended fusion valley can also be seen in Fig. 13 where, for fixed quadrupole moments, the PESs as a function of the octupole and hexadecapole moments are plotted. Again we can see the fusion valley even at low quadrupole moments. It extends towards much larger hexadecapole moments than shown in Figs. 4 and 5. This analysis provides one more, not very optimistic conclusion. Applying a triple constraint (on quadrupole, octupole, and hexadecapole moments) and preparing a three-dimensional surface in the self-consistent calculation explains most of the problems with discontinuities, but not all of them: even triple constraints does not guarantee the uniqueness of the solution. We can still obtain distinctly different shapes of the density distribution depending on the initial configuration.

IV. CONCLUSIONS

We have investigated the fission barriers of two heavy actinide nuclei, ^{252}Cf and ^{258}No, using the self-consistent microscopic approach. The calculations were made using multiple constraints on the quadrupole, octupole, and hexadecapole moments. A detailed analysis has shown a complicated structure of the potential-energy surface at large quadrupole deformations of the nucleus. The competition between local minima at a given quadrupole moment–compact, elongated, and symmetric elongated—determines the fission mode and the experimentally observed fragment mass distribution. We have shown that the scission may occur at a quadrupole deformation smaller than the one at the end of the fission path in the minimum of the valley on the potential-energy surface.

The calculations using three constraints give a much more complete description of the potential-energy surface. Nevertheless, it is possible to find distinct solutions of the HFB equations corresponding to the same values of the quadrupole, octupole, and hexadecapole moments. These configurations create various layers of the potential-energy surface in the same place of two- or three-dimensional maps. It makes the description of the fission even more complicated.

Reducing the full space of deformation to two dimensions creates a potential-energy surface that is not always continuous. Rapid changes of the configuration of density distribution may be found even at seemingly smooth surfaces. We therefore conclude that the jumps between surfaces must be discussed in the analysis of the fission process. This is especially relevant for subsequent analysis based on the time evolution of wave packets depending on the restricted set of collective coordinates. The influence of the discontinuities in such kind of calculations has to be investigated and carefully assessed. The discontinuities of the PES presented in this paper are an immanent property of the constrained calculations. Nevertheless, their existence usually does not affect the

analysis of the PES in two- or three-dimensional space. The possible jump between quite similar configurations has little impact on the conclusions extracted from the global analysis of the whole fission process.

In this paper, we are analyzing problems that appear when multidimensional energy (depending on the hundreds of thousands of parameters in the Bogoliubov transformation) is projected into a two- (or three-) dimensional picture based on standard deformation parameters. The energy as a function of the Bogoliubov parameters is a continuous function and it is only the projection on Q_{20}-Q_{30}, etc., that is causing the discontinuities in the energy as depicted as a function of those deformation parameters. Therefore our calculations satisfy the continuity requirement but only when all the independent parameters are considered.

The present analysis is based on the HFB approximation, but it also applies to any constrained, self-consistent type of calculations. Similar problems with multiple minima and surface discontinuities may also affect calculations made on a grid of fixed deformation parameters as in the macroscopic-microscopic models. In many papers, potential energy calculated in the multidimensional space of deformations is projected on two dimensions by finding minima of the energy with respect to the remaining deformation parameters (see, e.g., [8,9,11,12,17]). In this way, it is possible to visualize them as a map and discuss the obtained results in a more intuitive way. However, it might happen that there exist more than one local minimum of the energy in the multidimensional space of deformations for given coordinates on the map. In such a case, an unnoticed link between neighboring mesh points with similar energy but significantly distinct deformation may exist. Nevertheless, when the analysis is performed on a full, multidimensional grid of shape parameters, it is much easier than in self-consistent calculations to control the whole spectrum of nuclear shapes and to avoid uncontrolled configuration change.

We would like also to mention that the discussion of the determination of the potential-energy surface is not the only relevant issue in the analysis of fission. Many other aspects also have a significant impact on the dynamics of this process. We should mention here the influence of the inertia parameter and pairing degrees of freedom that shall also be investigated in the future.

[1] H. J. Krappe and K. Pomorski, *Theory of Nuclear Fission* (Springer, Berlin, 2012).

[2] N. Schunck and L. M. Robledo, Rep. Prog. Phys. **79**, 116301 (2016).

[3] M. Bender, R. Bernard, G. Bertsch, S. Chiba, J. Dobaczewski, N. Dubray, S. Giuliani, K. Hagino, D. Lacroix, Z. P. Li *et al.*, J. Phys. G: Nucl. Part. Phys. **47**, 113002 (2020).

[4] V. Pashkevich, Y. Pyatkov, and A. Unzhakova, Int. J. Mod. Phys. E **18**, 907 (2009).

[5] P. Möller, A. J. Sierk, T. Ichikawa, A. Iwamoto, R. Bengtsson, H. Uhrenholt, and S. Åberg, Phys. Rev. C **79**, 064304 (2009).

[6] M. Mirea, D. S. Delion, and A. Săndulescu, Phys. Rev. C **81**, 044317 (2010).

[7] H. Abusara, A. V. Afanasjev, and P. Ring, Phys. Rev. C **82**, 044303 (2010).

[8] A. N. Andreyev, J. Elseviers, M. Huyse, P. Van Duppen, S. Antalic, A. Barzakh, N. Bree, T. E. Cocolios, V. F. Comas, J. Diriken *et al.*, Phys. Rev. Lett. **105**, 252502 (2010).

[9] P. Möller, J. Randrup, and A. J. Sierk, Phys. Rev. C **85**, 024306 (2012).

[10] P. Jachimowicz, M. Kowal, and J. Skalski, Phys. Rev. C **85**, 034305 (2012).

[11] P. Jachimowicz, M. Kowal, and J. Skalski, Phys. Rev. C **87**, 044308 (2013).

[12] P. Möller, J. Randrup, A. Iwamoto, and T. Ichikawa, Phys. Rev. C **90**, 014601 (2014).

[13] B.-N. Lu, J. Zhao, E.-G. Zhao, and S.-G. Zhou, Phys. Rev. C **89**, 014323 (2014).

[14] R. Rodríguez-Guzmán and L. M. Robledo, Phys. Rev. C **89**, 054310 (2014).

[15] K. Pomorski, B. Nerlo-Pomorska, and P. Quentin, Phys. Rev. C **91**, 054605 (2015).

[16] R. Rodríguez-Guzmán and L. M. Robledo, Eur. Phys. J. A **52**, 348 (2016).

[17] C. Schmitt, K. Pomorski, B. Nerlo-Pomorska, and J. Bartel, Phys. Rev. C **95**, 034612 (2017).

[18] P. Jachimowicz, M. Kowal, and J. Skalski, Phys. Rev. C **95**, 014303 (2017).

[19] K. Pomorski, B. Nerlo-Pomorska, J. Bartel, and C. Schmitt, Phys. Rev. C **97**, 034319 (2018).

[20] Q.-Z. Chai, W.-J. Zhao, M.-L. Liu, and H.-L. Wang, Chin. Phys. C **42**, 054101 (2018).

[21] P. Jachimowicz, M. Kowal, and J. Skalski, Phys. Rev. C **101**, 014311 (2020).

[22] P. Jachimowicz, M. Kowal, and J. Skalski, At. Data Nucl. Data Tables **138**, 101393 (2021).

[23] R. Rodríguez-Guzmán, Y. M. Humadi, and L. M. Robledo, Eur. Phys. J. A **56**, 43 (2020).

[24] M. Verriere and D. Regnier, Front. Phys. **8**, 233 (2020).

[25] N. Dubray and D. Regnier, Comput. Phys. Commun. **183**, 2035 (2012).

[26] M. G. Urin and D. F. Zaretsky, Nucl. Phys. **75**, 101 (1966).

[27] L. G. Moretto and R. P. Babinet, Phys. Lett. B **49**, 147 (1974).

[28] J. Sadhukhan, J. Dobaczewski, W. Nazarewicz, J. A. Sheikh, and A. Baran, Phys. Rev. C **90**, 061304(R) (2014).

[29] S. A. Giuliani, L. M. Robledo, and R. Rodríguez-Guzmán, Phys. Rev. C **90**, 054311 (2014).

[30] R. Rodríguez-Guzmán and L. M. Robledo, Phys. Rev. C **98**, 034308 (2018).

[31] N. Schunck, D. Duke, H. Carr, and A. Knoll, Phys. Rev. C **90**, 054305 (2014).

[32] https://wwwndc.jaea.go.jp/cgi-bin/FPYfig?iso=sCf252 (2011).

[33] A. Göök, F.-J. Hambsch, and M. Vidali, Phys. Rev. C **90**, 064611 (2014).

[34] J. Weber, H. C. Britt, and J. B. Wilhelmy, Phys. Rev. C **23**, 2100 (1981).

[35] E. K. Hulet, J. F. Wild, R. J. Dougan, R. W. Lougheed, J. H. Landrum, A. D. Dougan, M. Schadel, R. L. Hahn, P. A. Baisden, C. M. Henderson *et al.*, Phys. Rev. Lett. **56**, 313 (1986).

[36] E. K. Hulet, J. F. Wild, R. J. Dougan, R. W. Lougheed, J. H. Landrum, A. D. Dougan, P. A. Baisden, C. M. Henderson, R. J. Dupzyk, R. L. Hahn *et al.*, Phys. Rev. C **40**, 770 (1989).

[37] G. Audi, F. G. Kondev, M. Wang, W. J. Huang, and S. Naimi, Chin. Phys. C **41**, 030001 (2017).

[38] J. F. Berger, J. D. Anderson, P. Bonche, and M. S. Weiss, Phys. Rev. C **41**, R2483(R) (1990).

[39] S. Péru and M. Martini, Eur. Phys. J. A **50**, 88 (2014).

[40] L. M. Robledo, T. R. Rodríguez, and R. R. Rodríguez-Guzmán, J. Phys. G: Nucl. Part. Phys. **46**, 013001 (2018).

[41] J. Berger, M. Girod, and D. Gogny, Comput. Phys. Commun. **63**, 365 (1991).

[42] M. Warda, J. L. Egido, L. M. Robledo, and K. Pomorski, Phys. Rev. C **66**, 014310 (2002).

[43] J.-P. Delaroche, M. Girod, H. Goutte, and J. Libert, Nucl. Phys. A **771**, 103 (2006).

[44] A. Baran, M. Kowal, P.-G. Reinhard, L. Robledo, A. Staszczak, and M. Warda, Nucl. Phys. A **944**, 442 (2015), Special Issue on Superheavy Elements.

[45] M. Warda and J. L. Egido, Phys. Rev. C **86**, 014322 (2012).

[46] S. Hilaire and M. Girod, Eur. Phys. J. A **33**, 237 (2007).

[47] S. Goriely, S. Hilaire, M. Girod, and S. Péru, Phys. Rev. Lett. **102**, 242501 (2009).

[48] L. M. Robledo and G. F. Bertsch, Phys. Rev. C **84**, 014312 (2011).

[49] J. Egido, L. Robledo, and R. Chasman, Phys. Lett. B **393**, 13 (1997).

[50] H. Goutte, J. F. Berger, P. Casoli, and D. Gogny, Phys. Rev. C **71**, 024316 (2005).

[51] A. Zdeb, A. Dobrowolski, and M. Warda, Phys. Rev. C **95**, 054608 (2017).

[52] A. Bulgac, S. Jin, K. J. Roche, N. Schunck, and I. Stetcu, Phys. Rev. C **100**, 034615 (2019).

[53] J. Randrup and P. Möller, Phys. Rev. Lett. **106**, 132503 (2011).

[54] I. Tsekhanovich, A. Andreyev, K. Nishio, D. Denis-Petit, K. Hirose, H. Makii, Z. Matheson, K. Morimoto, K. Morita, W. Nazarewicz *et al.*, Phys. Lett. B **790**, 583 (2019).

[55] M. Warda, A. Staszczak, and W. Nazarewicz, Phys. Rev. C **86**, 024601 (2012).

[56] M. Warda and L. M. Robledo, Phys. Rev. C **84**, 044608 (2011).

[57] M. Warda, A. Zdeb, and L. M. Robledo, Phys. Rev. C **98**, 041602(R) (2018).

[58] H. Britt, in *Physics and Chemistry of Fission 1979, Proceedings of the International Symposium on Physics and Chemistry of Fission, 14–18 May 1979, Jülich* (IAEA, Vienna, 1980), Vol. 1, p. 3.

[59] G. N. Smirenkin, Preparation of evaluated data for a fission barrier parameter library for isotopes with $Z = 82$–98, with consideration of the level density models used, IAEA International Nuclear Data Committee Report, INDC(CCP)-359, 1993, https://www-nds.iaea.org/publications/indc/indc-ccp-0359/.

[60] J. Zhao, B.-N. Lu, T. Nikšić, and D. Vretenar, Phys. Rev. C **92**, 064315 (2015).

[61] M. Wang, G. Audi, A. Wapstra, F. Kondev, M. MacCormick, X. Xu, and B. Pfeiffer, Chin. Phys. C **36**, 1603 (2012).

[62] A. Staszczak, A. Baran, J. Dobaczewski, and W. Nazarewicz, Phys. Rev. C **80**, 014309 (2009).

[63] A. Staszczak, A. Baran, and W. Nazarewicz, Phys. Rev. C **87**, 024320 (2013).

[64] M. Warda and A. Zdeb, Phys. Scr. **90**, 114003 (2015).

[65] D. Regnier, N. Dubray, and N. Schunck, Phys. Rev. C **99**, 024611 (2019).